Development of composite cements characterized by low environmental footprint

Gerd Bolte[1], Maciej Zajac[1], Jan Skocek[1], Mohsen Ben Haha[1]

[1] Global R&D, HeidelbergCement AG, Oberklamweg 2-4, 69181 Leimen, Germany

Abstract

The production of cement is associated with significant CO_2 emissions. The effective manner to cope with this challenge is the production of composite cements characterized by high Portland cement clinker replacement ratio. This contribution reports on the composition optimization of the ternary cement, with the purpose to maximize the cement performance evolution while minimizing its environmental impact. For this purpose, based on the understanding of the cement hydration and performance evolution, a modelling tool was developed allowing predictions of the compressive strength depending on the cement composition and curing time. The approach used accounted for the specific interactions among the Portland cement clinker, granulated blast-furnace slag and limestone and for the specific microstructure features in the investigate systems. The agreement between the predictions and performance evolution measured had confirmed the accuracy of the models developed as well as of the general concept of the composite cement optimization. Consequently, the effective global warming potential of the composite cements was calculated. This revealed that composite cements characterized by approximatively 50 wt.-% of Portland cement clinker, 40 wt.-% of granulated blast-furnace slag and 10 wt.-% of limestone are characterized by an appreciable performance and by the appreciably low environmental footprint.

Keywords (6)

Thermodynamic modelling, compressive strength, porosity, ground granulated blast-furnace slag, limestone, warming potential

1. Introduction

Cement industry is one of the largest manufactures of goods on Earth by mass, providing the building materials that are easily accessible word wide. Unluckily, the cement production is associated with significant CO_2 emissions (Salas et al., 2016; Scrivener et al., 2018). Since the demand for building materials and particularly for the cement is increasing, the CO_2 emissions would further increase negatively contributing to the climate changes, under business-as-usual scenario (Scrivener et al., 2018). The cement industry has already reached significant reductions of CO_2 emissions associated with the cement production. This has been achieved over the increased energy efficiency, use of alternative fuels and through Portland cement clinker substitution by supplementary cementitious materials (SCMs). These efforts need to be further followed to cope with the increasing cement demand. Particularly, the rate of the SCMs used as partial replacements for Portland cement clinker (herein "clinker") needs to be increased (Scrivener et al., 2018; Gartner and Hirao, 2015). Currently, the most suitable SCMs are semi-hydraulic or pozzolanic materials such as granulated blast-furnace slags (herein "slag") and coal fly ashes (Scrivener et al., 2018; Lothenbach et al., 2011). The availability of these materials with adequate quality is limited to only about 20 wt.-% of global cement production and are unlikely to increase (Scrivener et al., 2018). Application of another known SCM, limestone, is limited because of its little contribution to the cement performance (De Weerdt et al., 2011). Thought, recent research work revealed that use of slag

and fly ash together with limestone may lead to the further increase of the clinker replacement ratio (Schöler et al., 2017; Adu-Amankwah et al., 2017b).

HeidelbergCement launched a research program aiming at understanding of parameters that allow the maximization of the cement clinker replacement by slag and limestone while meeting an adequate cement performance. An additional target of these investigations was to limit the amount of slag. This goal was achieved over the understanding of the interactions among the reacting clinker, slag and limestone in cement (Adu-Amankwah et al., 2017b; Bolte and Zajac, 2016) accompanied by the development of the optimal production methods for the composite cements. These efforts have led to establishing the know-how supported by the modelling tools (Zajac and Ben Haha, 2014; Skocek et al., 2017; Zajac et al., 2018) allowing the optimization of the cement composition and properties.

This contribution presents the numerical models for the optimization of the multicomponent cements. The modelling results are validated in the cement mortars against the available literature data. Additionally, the performance of the optimal compositions are verified in concrete.

2. The model

The optimization procedure applied within this work comprises several numerical models. Results obtained at each calculation step constitute the input for the next step. By combining an empirical model that describes the dissolution of the clinker phases with a thermodynamic equilibrium model that assumes equilibrium between the solution and the hydrates together with an empirical model relating the porosity with the strength, the evolution of the compressive strength can be linked to the initial cement composition and time from mixing with water. Additionally, the intermediate modelling results may be used as an indication of the durability performance (Kunther et al., 2013; Whittaker et al., 2016) and may facilitate explanation of the phenomena observed. The here described approach is derived from the modeling approaches developed in (Lothenbach and Winnefeld, 2006) and further improved in (Skocek et al., 2017).

The modelling of the compressive strength evolution as a function of the cement composition and time is based on the:

- Definition of the composite cement composition, including the composition of the clinker and supplementary cementitious materials
- Calculation of the reactive phases dissolution kinetics
- Thermodynamic calculations using a consistent thermodynamic dataset to predict the porosity
- Calculation of the compressive strength based on the predicted porosity

Consequently, the global warming potential of the investigated composite cements was compared to the calculated compressive strength to verify the “environmental efficiency” of the investigated systems.

In the next section, the reader finds the detailed description of each modelling step.

2.1. Materials and Composition

Basic characteristics of the clinker, slag and limestone are given in this section. The compositions in the following ranges were investigated: 50 – 100 wt.-% clinker, 0 – 50 wt.-% slag and 0 – 50 wt.-% limestone.

Composite cements were made from a commercial Portland clinker with its typical composition (see Table 1), ground granulated blast-furnace slag and ground natural limestone (see Table 2). All the materials were

produced or quarried in Germany. For the calculations, it was assumed that the slag and limestone contain only glassy phase and calcite, respectively. The overall SO_3 level was set to 3 % by adding calcium sulfate (anhydrite).

The modelled compositions are given in Figure 1.

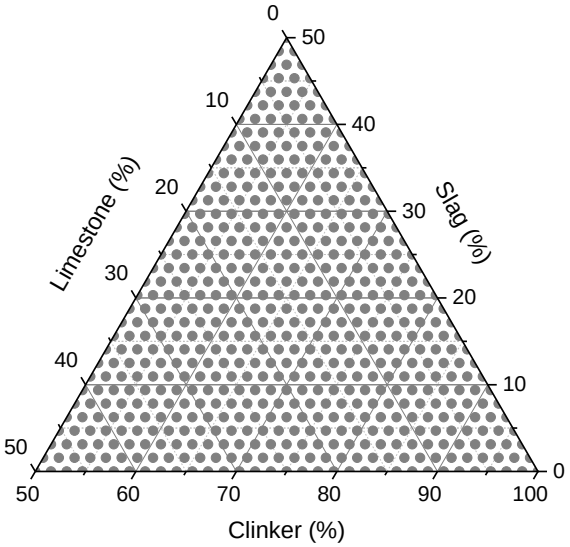

Figure 1 Modelled compositions of cements

Table 1 Clinker content of CEM I 52.5R (wt.-%)

Phase	Alite	Belite	Aluminate	Ferrite	Calcite	Anhydrite	Basanite	Others
CEM I	58.1	14.3	9.2	6.7	1.9	1.7	3.0	5.1

Table 2 Mineralogical composition of supplementary materials (wt.-%)

Phase	Calcite	Quartz	Dolomite	Anhydrite	Amorphous/Others
Slag	2.4	0.1	-	-	97.5
Limestone	96.6	0.4	1	-	2.0
Quartz	0.5	99.5	-	-	-
Anhydrite	-	2.1	5.5	91.0	1.4

2.2. Kinetics of reaction

Multi-parametric smooth functions were used to idealized the reaction of the anhydrous phases in time. These curves were fitted to experimental data published in our earlier studies (Adu-Amankwah et al., 2017b; Whittaker et al., 2014) as well on the other available literature data (Kocaba et al., 2012; Berodier

and Scrivener, 2015) . The composition of the materials used within these studies were similar to the investigated earlier (Adu-Amankwah et al., 2017b; Whittaker et al., 2014).

The kinetics of the reaction of the slag was modified according to the results of Adu-Amankwah (Adu-Amankwah et al., 2017b) and Berodier (Berodier and Scrivener, 2015). The reaction of slag is inversely proportional to its content in the composite cement. Berodier has demonstrated that an increase of the slag content from 10 to 30 wt.-% resulted in the limitation of the slag reaction by about 25 wt.-%. Similar results are presented in the work of Adu-Amankwah et al. (Adu-Amankwah et al., 2017b), thought the changes related to the decrease of the slag content from 50 to 30 wt.-% resulted in the slag reaction increase by only 10 % at hydration times between 7 and 180 days. The differences can be explain in the different water to cement ratio (w/c) used in these studies: in Berodier (Berodier and Scrivener, 2015) it was mainly w/c = 0.40 while Adu-Amankwah (Adu-Amankwah et al., 2017b) used 0.50. Since at the later hydration times, the slag hydration is mainly limited by the available space (Berodier and Scrivener, 2015), the higher water to cement ration reduces the impact of the slag content on its reaction kinetics. Consequently, the kinetics of the slag reaction was fitted as in the work of (Adu-Amankwah et al., 2017b; Whittaker et al., 2014) for the cements containing 40 – 50 wt.-% of the slag at w/c = 0.50. The slag reaction was used to decrease linearly with its content. The difference amounted for 25 % between 0 and 50 % slag at the end of hydration (Figure 2).

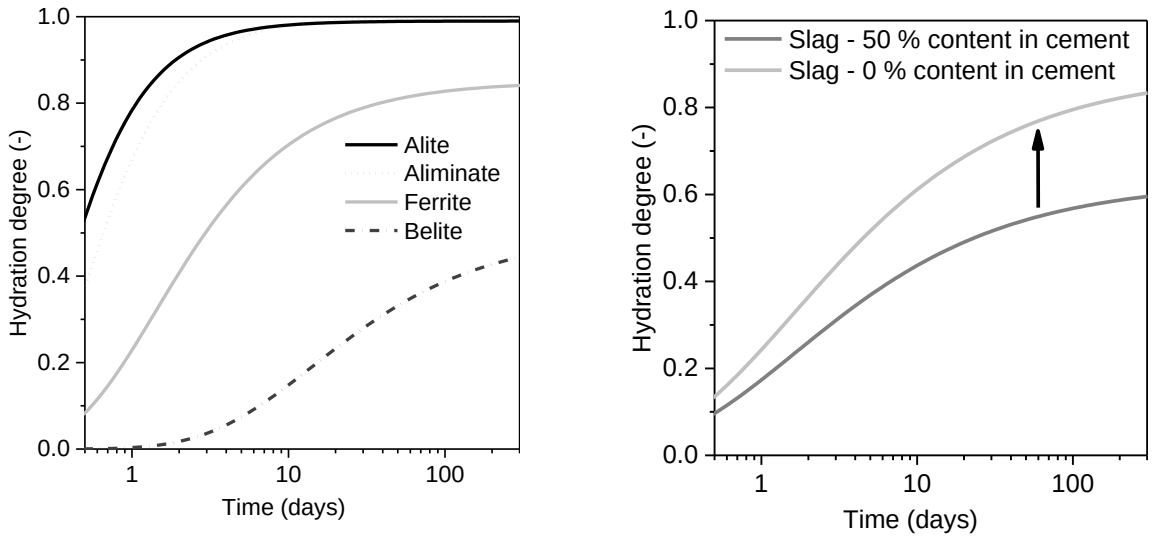

Figure 2 Hydration degrees of the clinker (left) and slag (right) fitted to the measured data in (Adu-Amankwah et al., 2017b; Zajac et al., 2018). The slag hydration degree was fitted for the content of the slag of 50 wt.-%. For the lower slag content the hydration of the slag was model to increases according to the data in (Zajac et al., 2018; Berodier and Scrivener, 2015). The arrows indicate the increases of the reaction degree of slag as a result of the decreasing slag content in cement.

The hydration degree of the clinker phases is modified to lower extend when compared to the hydration degree of the slag, when changing the composition of the cement (Adu-Amankwah et al., 2017b; Berodier and Scrivener, 2015). Consequently, it was kept constant independently from the cement composition.

The hydration kinetics were fitted to the data shown in (Adu-Amankwah et al., 2017b; Zajac et al., 2018) (Figure 2).

2.3. Thermodynamic model

Thermodynamic modeling was applied to compute the composition of hydrated cementitious matrix at different hydration times. This allowed for calculating the evolution of the total pore volume (Damidot et al., 2011). Calculations were carried out by means of the geochemical modelling program GEMS (Gibbs Energy Minimization Software) (Kulik et al., 2013; Wagner et al., 2012). The thermodynamic data were from the PSI-GEMS database (Wolfgang Hummel et al., 2002; W Hummel et al., 2002). Additionally, the data base was extended by the cement specific data (Lothenbach et al., 2018).

When modelling, the clinker phases, slag and calcium sulfate were dissolved congruently. Consequently, their reaction degree emerged from the thermodynamic equilibrium and particularly it is limited by the available alumina. Currently, the available model does not allow for the calculating the Al incorporation in C-S-H phase. The modelled phase composition was modified with Al incorporation following the C-S-H phase composition determined experimentally (Adu-Amankwah et al., 2017b; Whittaker et al., 2014).

2.4. Prediction of the compressive strength

The knowledge of the volume of hydrates and anhydrous materials enables the calculation of porosity at a given hydration time (Zajac et al., 2018):

$$\boldsymbol{P(t)} = (\mathbf{1} - \frac{\boldsymbol{V_{Anhydrous}(t)+V_{Hydrates}(t)}}{\boldsymbol{V_{water}+V_{initial\ cement}}}) \times \mathbf{100}\% \qquad \textbf{Eq. 1}$$

where P(t) is the pore volume at time t, V_{water} is the volume of the mixing or free water, $V_{initial\ cement}$ is volume of cement before reaction, $V_{Anhydrous}(t)$ is volume of unreacted cement, $V_{hydrates}(t)$ is volume of hydrates. The porosity calculated by the thermodynamic model was used for the calculation of the prediction of the strength depending on the cement composition and the hydration time as

$$\boldsymbol{R_c(t)} = \mathbf{3.7}\ \boldsymbol{P(t)}^{\mathbf{-6.2}} \times \mathbf{10^{10}} \qquad \textbf{Eq. 2}$$

where $R_c(t)$ is the compressive strength in MPa at time t. Equation 2 is a fit of data presented in Figure 3.

Within the present work, a simple relationship between the porosity and the compressive strength was assumed. The relationship was fitted for the data presented in (Zajac and Ben Haha, 2014) and in (Zajac et al., 2018). In the earlier work, we have shown that there is no unique relationship between the porosity and strength (or between the gel-space ratio and the strength) for the neat cements and the composite cements (Skocek et al., 2017; Zajac et al., 2018). However, this can be corrected by adjusting the density of the C-S-H phase as demonstrated for neat Portland cements (Lothenbach et al., 2008b) composite cements containing slag (Zajac et al., 2018) (Kucharczyk Sylwia et al., 2016; Ishida et al., 2011) and fly ash (Zajac and Ben Haha, 2014; Termkhajornkit and Nawa, 2007). Following the results of (Zajac et al., 2018), the density of C-S-H was reduced to 2.0 g/cm^3 in the composite cements for replacement ration of 50 wt.-%. In the plain Portland cement paste, the density of C-S-H was 2.4 g/cm^3, as given by GEMs. The simple linear relationship between the density and the clinker content in cement was assumed, since no reliable data exist for different replacement ratios (Figure 4). This concept reflects the difference in the microstructure development between the neat cement and composite cements, i.e.: better filling capacity of the composite cements discussed in the previous paragraph (Lothenbach et al., 2011).

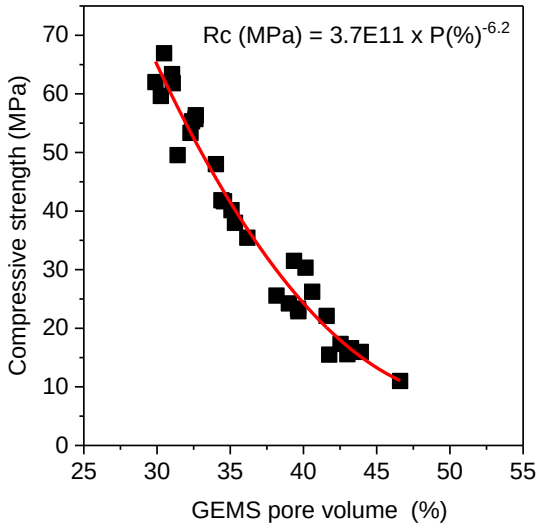

Figure 3 Comparison between measured compressive strength and porosity volume calculated by GEMS, data from (Zajac et al., 2018). The equation in the graph is a fit of the data depicted by the red line. In the equation, Rc is the compressive strength and P the GEMS pore volume.

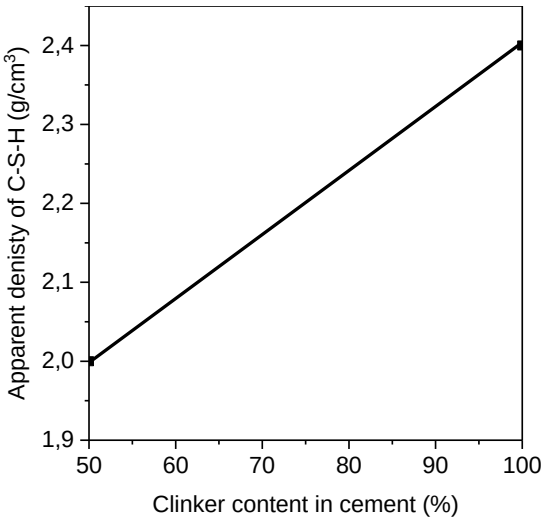

Figure 4 Apparent density of C-S-H used for the modelling of the compressive strength of the cements with different compositions.

Although the correlation between the strength and porosity as well as the correction of the C-S-H phase density is only empirical and does not explain the generic mechanisms, it was demonstrated that it is suitable for the prediction of the compressive strength without explaining underlining mechanisms.

2.5. CO_2 balance (global warming potential)

Within this work, the potential to reduce the CO_2 emission associated with the cement production was evaluated using a simplified analysis. The CO_2 emissions associated with the materials were taken from The Cement Sustainability Initiative WBCSD-CSI ("The Cement Sustainability Initiative," 2017) tool for Environmental Product Declarations (EPDs) of concrete and cement (v1.4) ("The Cement Sustainability Initiative Environmental Product Declaration (EPD)," 2017), based on Eco invent (v3.3) ("The ecoinvent Database," 2017).

Global warming potential (GWP_{CO_2eq}) takes into account the contribution of CH_4, NO_x, SO_x, CO_2 gases emitted during production of the material, including: excavation, manufacturing and transport. The GWP_{CO_2eq} was calculated using equation (Maddalena et al., 2018):

$$\boldsymbol{GWP_{CO_2eq}} = \sum \boldsymbol{n_i}\left(\boldsymbol{d_i} \cdot \boldsymbol{t_{iCO_2eq}} + \boldsymbol{p_{iCO_2eq}}\right) \quad \textbf{Eq. 3}$$

Where n_i is the fraction of component, d_i transportation distance, t_{iCO_2eq} is the emission for the transportation and p_{iCO_2eq} is emission associated with the production process.

The scenario investigated was for cement plant located in a central European country. The emission associated with the clinker production was calculated to be 799 $kgCO_{2eq}/t_{clinker}$. This includes clinker manufacturing and grinding. For the slag, calculations were performed when assuming the following input: granulation of the slag requires 71.3 MJ/t, transport by a truck over 100 km, drying (0.22 GJ/t energy for drying and 14 kWh/t for all mechanical treatments) and grinding of the slag 87 kWh/t. This gives the

emissions associated with the ready to use slag of 85 $kgCO_{2eq}/t_{slag}$. In the case of limestone, the processes considered comprise transport over 3 km and grinding (10 kWh/t) giving 8 $kgCO_{2eq}/t_{limestone}$ ready to use for the cement production. The mixing of components as well as the calcium sulfate quarrying and grinding were not assumed in the calculation. This is because the contribution of these is the same in the investigated here composition range and the contribution of both is limited in the overall picture.

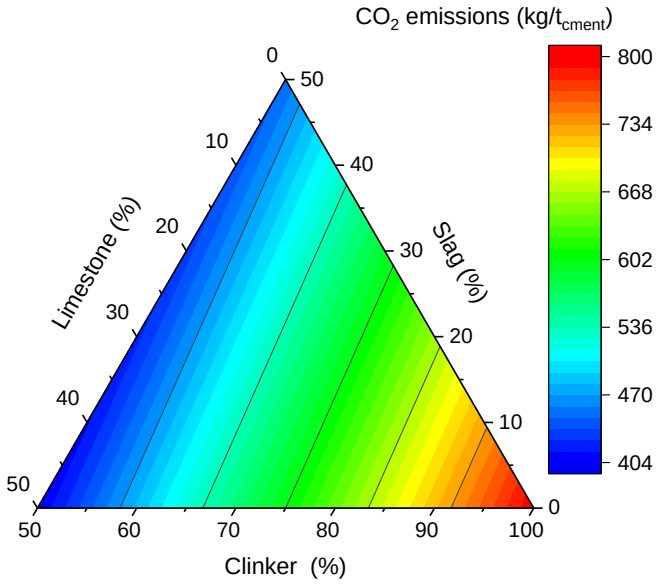

Figure 5 Specific CO_2 (global warming potential) emissions for the composite cements depending on the cement composition.

The results of the calculated CO_2 specific emissions (global warming potential) depending on the cement compositions are given in Figure 5. The graph shows the principle concept of the CO_2 reduction over the clinker replacement by SCMs to save cement production associated CO_2 emissions. Since the global warming potential for the clinker is significantly higher than for the slag and limestone, the replacement of the clinker by the both SCMs brings a significant reduction of the emissions.

3. Results and discussion

3.1. Modelling results

The cement composition has a pronounced impact on the content of these phases and consequently on the formed microstructure and performance (Lothenbach et al., 2011; Zajac et al., 2018). Modelling predicts the formation of the C-S-H phase, portlandite and ettringite in all composition range investigated. Depending on the limestone presence AFm phases (i.e. monosulfate, hemicarbonate and monocarbonate) composition vary. In the presence of limestone monocarbonate is calculated, while in limestone free system monosulfate is expected to precipitate (Adu-Amankwah et al., 2017b; Whittaker et al., 2014). Additionally, hydrotalcite and hydrogarnets precipitate. However, their content is significantly lower (Adu-Amankwah et al., 2017b; Whittaker et al., 2014).

These impacts of cement compositions on hydrates assemblage are described in detail at the hydration times of 28 days. Figure 6 shows the content of the AFm phases, ettringite, portlandite and C-S-H phases

for the compositions studied. Understanding of these impact is of a primary importance because the phases formed govern the porosity and hence the resulting strength performance (Zajac et al., 2018).

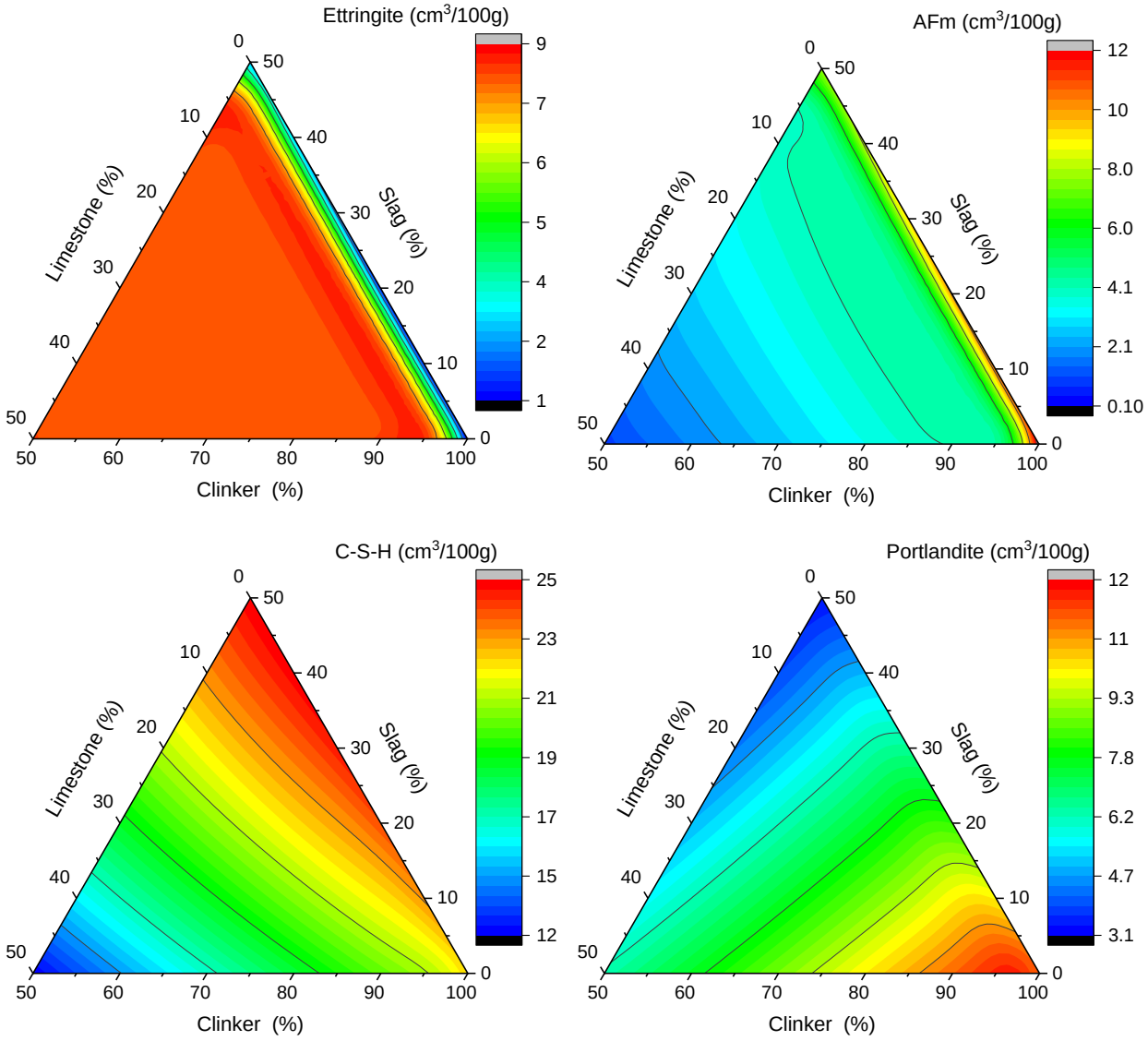

Figure 6 Effect of the cement composition of the content of the main hydrates at 28 days of hydration

Limestone blends with alumosilicate-bearing SCMs and clinker are characterized by complex interactions between its constituents. In such type of composite cements, calcite from limestone reacts with the available alumina from the clinker and slag to form monocarboaluminate phases instead of the monosulfoaluminate phase present in cements without limestone (De Weerdt et al., 2011; Adu-Amankwah et al., 2017b; Zajac et al., 2014). This results in ettringite stabilization, decreased porosity and increased strength. The adopted modelling method fully describes these interactions between alumina bearing phases and limestone present and provides further insights. Figure 6 reveals that ettringite content initially increases with the increasing content of limestone (calcite). Additionally, modelling reveals that this is accompanied by the transformation of monosulfate to monocarbonate as described

above (results not shown). The ettringite content stays constant from a calcite content of about 5 wt.-%, further increase of calcite content does not promote the formation of any additional ettringite. Figure 6 gives as well the total content of AFm phases, i.e. the sum of monocarbonate and monosulfate. These are the highest for the high clinker and the lowest slag contents and continuously decrease with increasing calcite content. These both phenomena, i.e. the stable ettringite content and decreasing AFm phases content from 2 – 5 wt.-% limestone, are explained by the impact of the cement composition on the alumina balance. When the content of calcite increases, the available alumina content decreases, i.e. alumina from dissolved clinker and slag, at given hydration time. Since the ettringite is thermodynamically more stable than AFm phases, there is less and less available alumina to form AFm phases. Note that in investigated composite cements, significant portion of alumina is located in the C-S-H phase (Lothenbach et al., 2011; Adu-Amankwah et al., 2017b; Whittaker et al., 2014) and the sulfate content in the investigated systems is kept constant. Consequently, the systems rich in limestone are virtually free from AFm phases.

Portlandite is formed from the hydration of clinker. In slag containing composite cements, a part of portlandite is consumed to from hydrates such as AFm and C-S-H phases (Lothenbach et al., 2011). This interplay is fully captured by the model (Figure 6). The maximal portlandite content is predicted to be present in the neat Portland cement. The increasing slag content results in a higher decrease of portlandite content when compared to the impacts of limestone. The C-S-H phase content is the highest for the compositions rich in clinker and slag. It is noticeable that already at 28 days of hydration, the contribution of the slag is significant so that the highest C-S-H phase content is found for the samples rich in slag. The increasing limestone content reduces the C-S-H phase content. Thought, because of the slag contribution the blends containing 40 wt.-% of slag and 10 wt.-% of limestone are characterized by the higher C-S-H content than the pure Portland cement at 28 days.

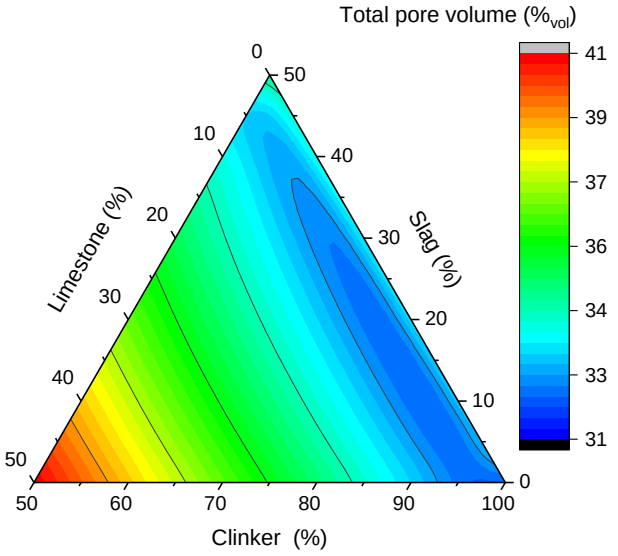

Figure 7 Calculated porosity at 28 days of hydration

The resulting porosity is plotted in Figure 7. The lowest porosity is calculated for the systems rich in clinker and the slag. The positive effect of the calcite and alumina bearing phases (De Weerdt et al., 2011; Adu-Amankwah et al., 2017b; Zajac et al., 2014; Schöler et al., 2015) is visible; the lowest porosity is registered for the samples characterized by about 5 wt.-% of limestone and up to 30 wt.-% of slag. The increase of the slag content to more than 30 wt.-% results in the increase of the porosity. This indicates that the increasing C-S-H volume is not able to compensate for the decrease of the other hydrates, e.g. portlandite. The increase of the limestone content to more than about 5 wt.-% results always in the pore volume increase.

The predicted compressive strength is shown in Figure 8 at three hydration times: 7, 28 and 180 days. The early compressive strength is dominated by the content of the clinker. The higher the clinker, the higher is the compressive strength. This observation is related to the kinetics of the reaction of the different materials. As shown in Figure 2, the clinker phases (particularly C_3S and C_3A) react faster than slag. Thus, at the early times, mainly the reaction of the clinker contributes to the formation of the microstructure and resulting compressive strength. However, it is noticeable that already at that time some small presence of limestone has a positive impact on the compressive strength according to the mechanisms described in (De Weerdt et al., 2011; Lothenbach et al., 2008a).

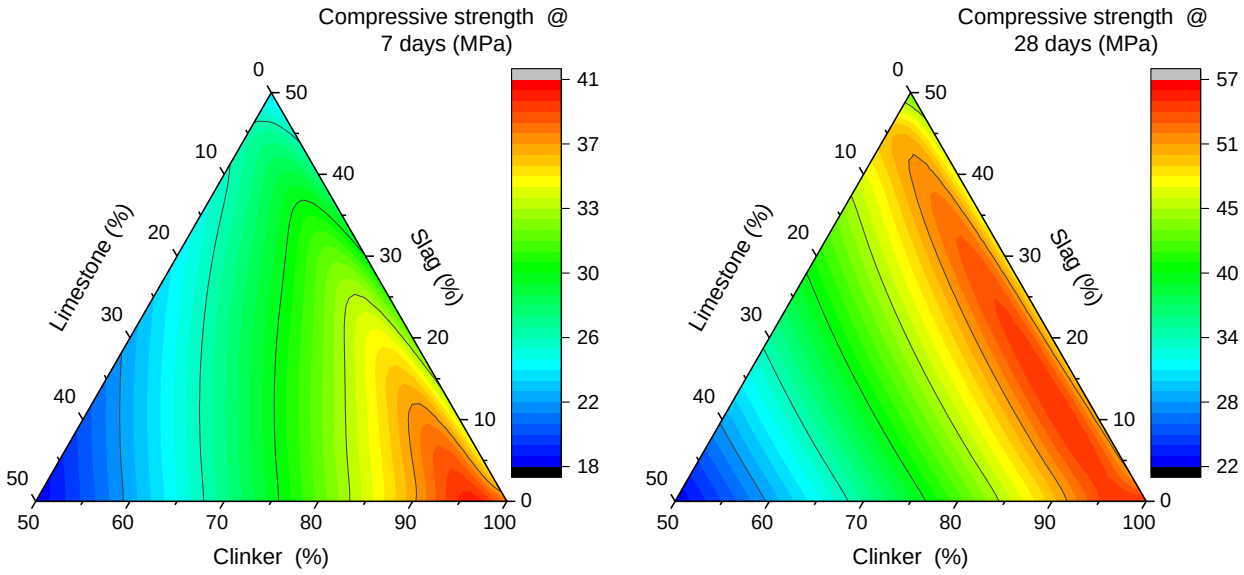

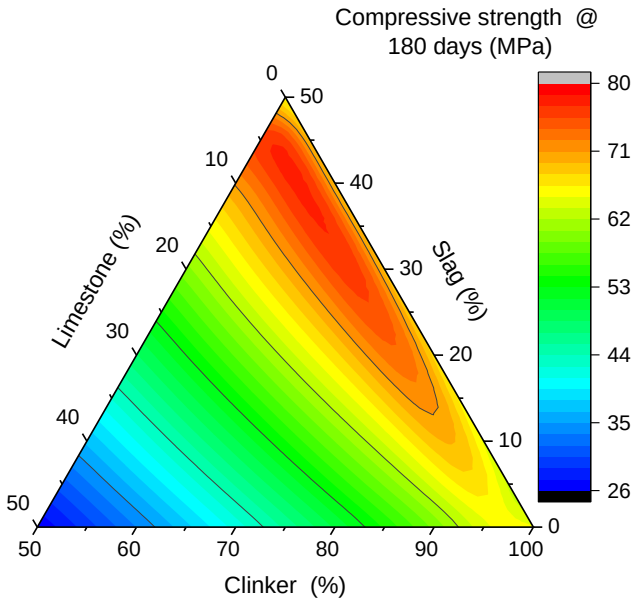

Figure 8 Predicted compressive strength at 7, 28 and 180 days of hydration

At 28 days of hydration, the contribution of the slag is clearly pronounced. The highest compressive strength is visible for the cements containing between 0 and 30 wt.-% of slag. Further increase of the slag content results in a reduction of the compressive strength since the relatively low reaction degree of the slag at 28 days is not able to compensate for the dilution of the cement clinker. However, at 180 days of hydration, the highest compressive strength is predicted for the system rich in slag, even if overall hydration degree is lower, when compared to the pure Portland cement (compare to Figure 2). This phenomenon is related to the fact that the slag containing blends are characterized by a more efficient microstructure from the perspective of the strength formation, when compared to the pure Portland cement (Zajac et al., 2018).

For all investigated cements, the increase of the limestone content by more than ~ 10 wt.-% results in the decrease of the compressive strength (De Weerdt et al., 2011; Zajac et al., 2018; Lothenbach et al., 2008a). Limestone contributed only limited to the formed microstructure by interacting with alumina bearing phases.

The effective global warming potential was calculated as the global warming potential in kg of CO_2 that needs to be emitted to produce the cement of a given compressive strength:

$$\boldsymbol{GWP_{Eff}(\mathrm{kg/MPa}) = \frac{GWP}{Rc(t)}} \quad \textbf{Eq. 4}$$

where GWP_{Eff} is the effective global warming potential, GWP is the warming potential of the cement of a given composition as shown in section "CO_2 balance" Figure 5 and Rc(t) is calculated compressive strength for a given cement composition at given hydration time (Figure 8). The results of these calculations are shown in Figure 9.

It is noticeable that despite the important relation between the cement composition and the resulting strength (Figure 8), the effective global warming potential is the lowest for the systems characterized by the high slag and limestone content at all hydration times.

The slag is an effective mean to reduce the global warming potential of the cement. It is associated with the low global warming potential and contributes to the compressive strength significantly. Despite the

fact that limestone does not contribute significantly to the strength, it significantly reduces the global warming potential of cement. Consequently, it has a significant impact on the effective global warming potential. Thought, when the limestone content is higher than about 25 %, the effective global warming potential is similar to the pure Portland cement or even higher. This is related to the very strong reduction of the compressive strength.

Consequently, there is an optimal content of the limestone from the perspective of the strength evolution and global warming potential, contrary the increase of the slag content at the adopted scenarios, results always in the reduction of the effective global warming potential.

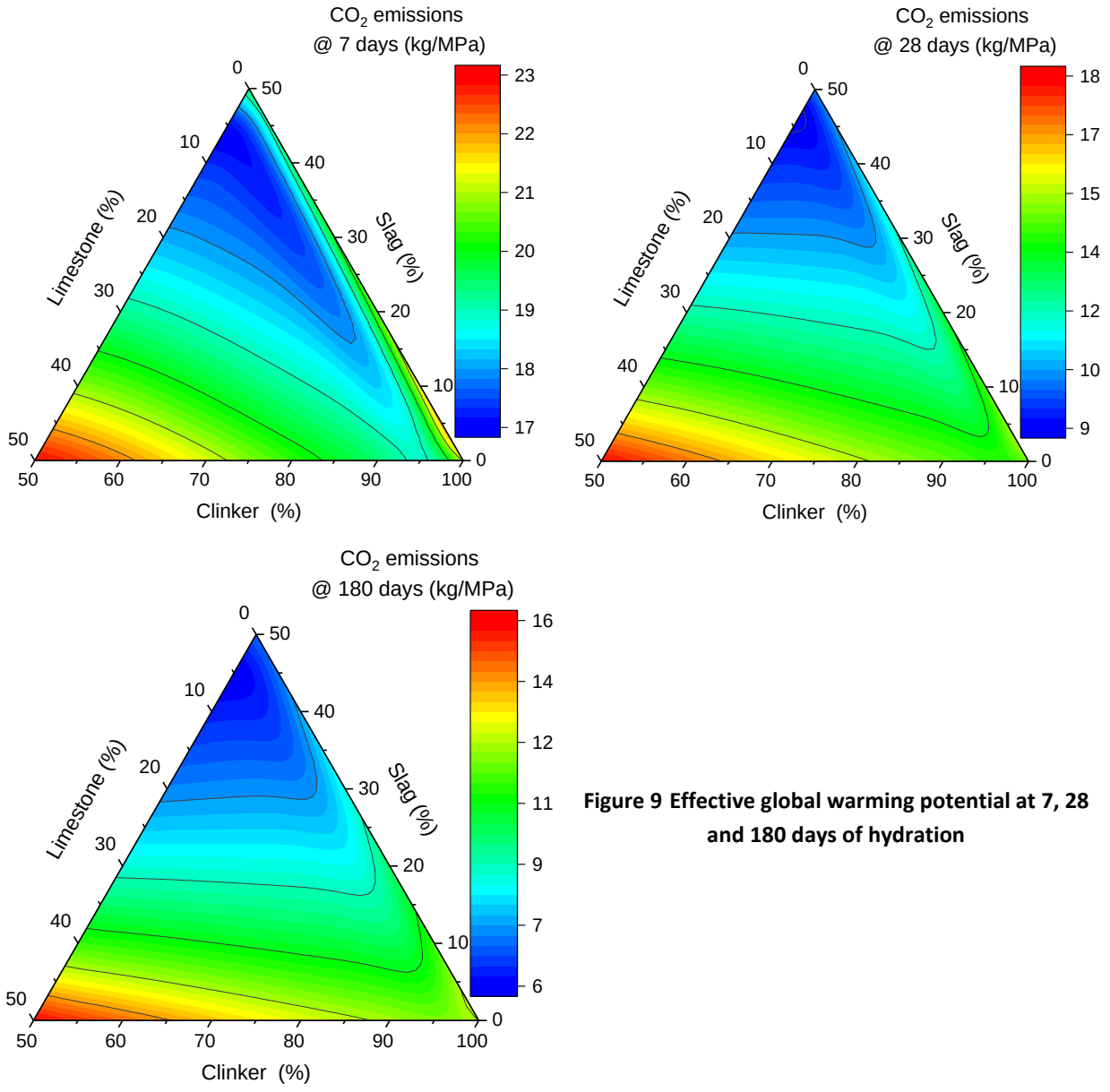

Figure 9 Effective global warming potential at 7, 28 and 180 days of hydration

3.2. Results validation in mortar

Antoni et al. (Antoni et al., 2015) investigated the performance evolution of the ternary mixes made of clinker, slag and limestone in the compositional range similar to the investigated within this work. They have reported the 2, 7 and 28 days compressive strength results for 23 different ternary compositions, containing up to 50 wt.-% limestone and slag. The cements were prepared in the laboratory by blending the cement components in a laboratory mixer. The experimental conditions were as well similar to the investigation used for the calibration of the modelling (Adu-Amankwah et al., 2017b; Zajac et al., 2018). Mortar bars were cast according to EN 196-1 procedure, at constant w/c of 0.50. Standard sand was used in all mortar mixes. The results of the strength measurements are re-plotted in Figure 10.

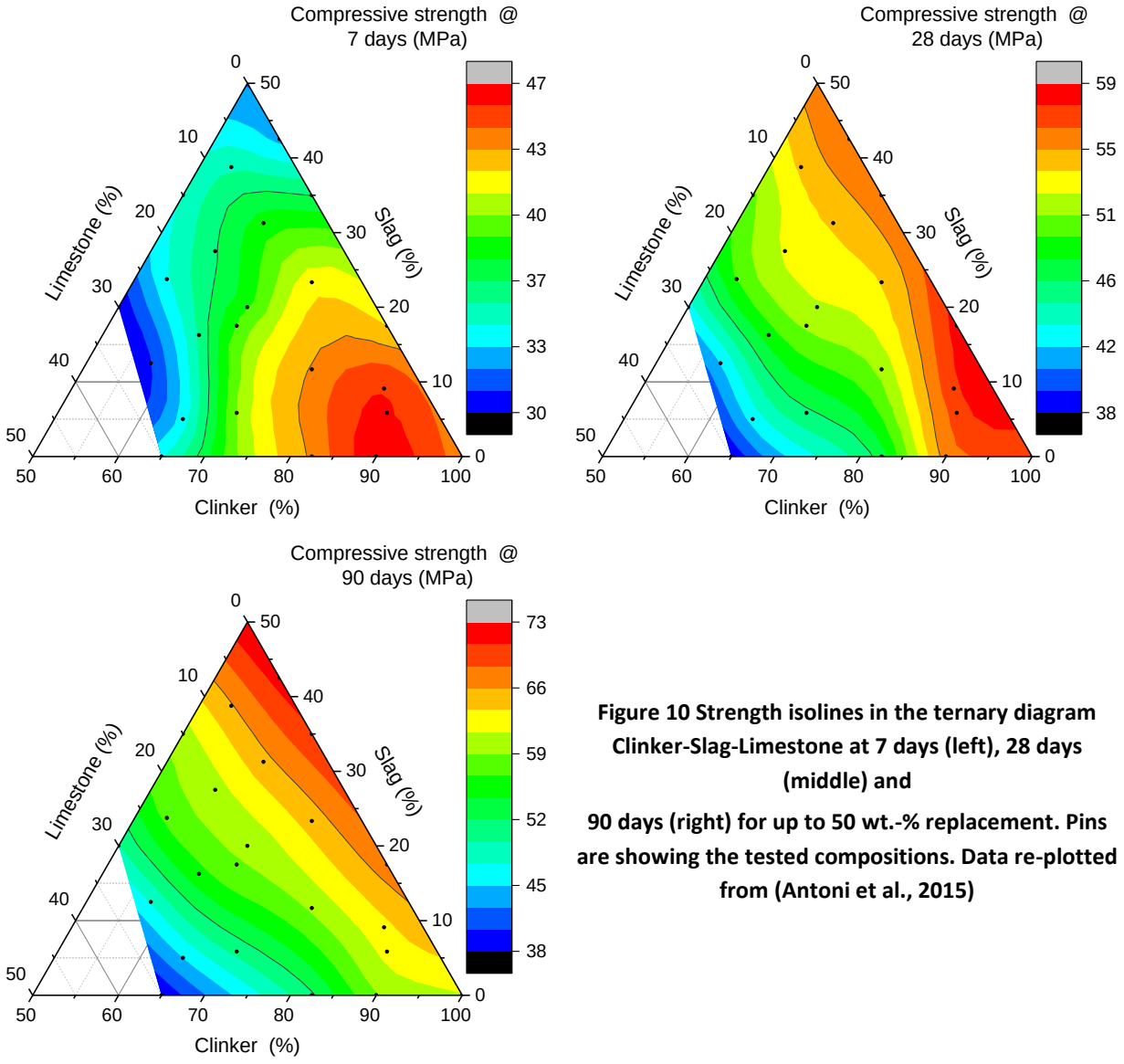

Figure 10 Strength isolines in the ternary diagram Clinker-Slag-Limestone at 7 days (left), 28 days (middle) and

90 days (right) for up to 50 wt.-% replacement. Pins are showing the tested compositions. Data re-plotted from (Antoni et al., 2015)

At early hydration times the slag and limestone mostly dilutes the clinker and consequently the strength decreases. Improvement of the strength is noticeable for the low limestone contents. With the increasing time from mixing with water, the contribution of the slag increases.

The measured compressive strength trends match very well the compressive strengths predicted by the here adopted modelling approach. The measurement data do not capture, however, the positive impact of limestone at all hydration times. While the measurements data are collected for limited range of the composition, the modelling tools provide significantly higher resolution and are hence capable to precisely find the optimal compositions.

This comparison confirms that adopted modelling approach can correctly account for the interactions in the reacting multicomponent cement, microstructure features and consequently it correctly predicts the compressive strength evolution.

3.3. Performance in concrete

As discussed, the compressive strength of the composite cement can be optimized reflecting as well their environmental footprint. Though, an open field that needs more study is the durability behavior, especially of the compositions characterized by the lower clinker content. The predictive models for the concrete performance do not exist yet (Alexander and Thomas, 2015; Hooton, 2015).

In order to verify the performance of the composite cements, the laboratory blended cements were tested in concretes. The tested cements are characterized by the clinker replacement ratio of 60 and 50 wt.-%, respectively, and contain 10 wt.-% of limestone. These blends are the most effective form the perspective of the effective global warming potential (Figure 9) at 28 days and have an appreciable performance (Figure 8). In order to prepare these cements, industrial CEM I 52.5 R was mixed with the ground slag and ground limestone and calcium sulfate. Additionally, commercially available reference composite cements, which are well established on the European market, were investigated (e.g. for Germany (VDZ-Publikation, 2017) these are CEM II/A-S and CEM II/A-LL and CEM III/A). The composition of the tested cements is given in Table 3. The target strength class of the cement was 42.5 as defined by the EN 196-1 norm, and comparable to the average strength level on the German market.

Table 3 Composition of the cements used for the concrete preparation (wt.-%), following the definitions of EN 197-1

	clinker	slag	limestone	SO_3
LabCEM1	60	30	10	2.9
LabCEM2	50	40	10	2.9
CEM II/A-S 42.5 R	82	18	-	3.0
CEM II/A-LL 32.5 R	82	-	18	3.2
CEM III/A 42.5 N	60	40		2.8

The following concrete performances were tested: evolution of the compressive strength, carbonation resistance, resistance of the concrete to the chloride attack and freeze-thaw resistance. The detailed description of the methods is given in appendix. The composition of the concretes is given in **Fehler! Verweisquelle konnte nicht gefunden werden.** in Appendix.

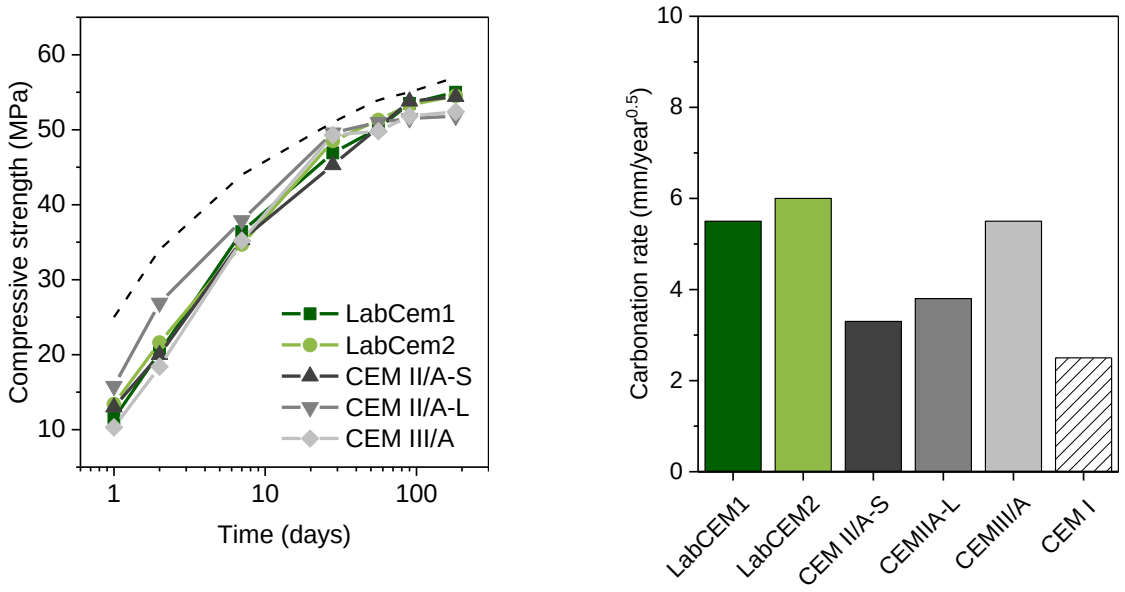

Figure 11 Concrete strength evolution and carbonation rates. Additionally, the dashed line shows the strength results for concrete based on CEM I 52.5 R used for the preparation of the LabCems, the carbonation results are given for the same CEM I 52.5 R.

The compressive strength evolution of the concretes is given in **Fehler! Verweisquelle konnte nicht gefunden werden.**. The compressive strength of the two investigated laboratory made cements is similar to the currently commercially available CEM II/A-S and CEM III/A of the same strength class. However the strength is initially lower when compared to the cement CEM II/A-LL. At 90 days from mixing with water, all the cement are characterized by the same compressive strength.

The carbonation rates are presented in **Fehler! Verweisquelle konnte nicht gefunden werden.**-right. The rates are inversely proportional to the clinker content of the cements. The carbonation rates of optimized composite cements are comparable to the commercial CEM III/A and higher than the investigated CEM I and CEM II cements.

The resistance of the concretes to the freeze-thaw without de-icing salt was examined. The results of the scaling and the relative modules of elasticity evolution during the freeze-thaw test (CIF) are plotted in Figure 12. The concrete samples based on the cement containing slag are characterized by the similar performance. All these concretes had a relative modules of elastic > 75 % after 28 cycles fulfilling the acceptance criterion according to German requirements (für Wasserbau, 2012). What is surprising is that the concrete based on the commercial CEM II/A-LL has failed to meet this criterion. The scaling during the CIF test was significantly below the limit of 1000 g/m^2 after 56 freeze-thaw cycles as given in (für Wasserbau, 2012).

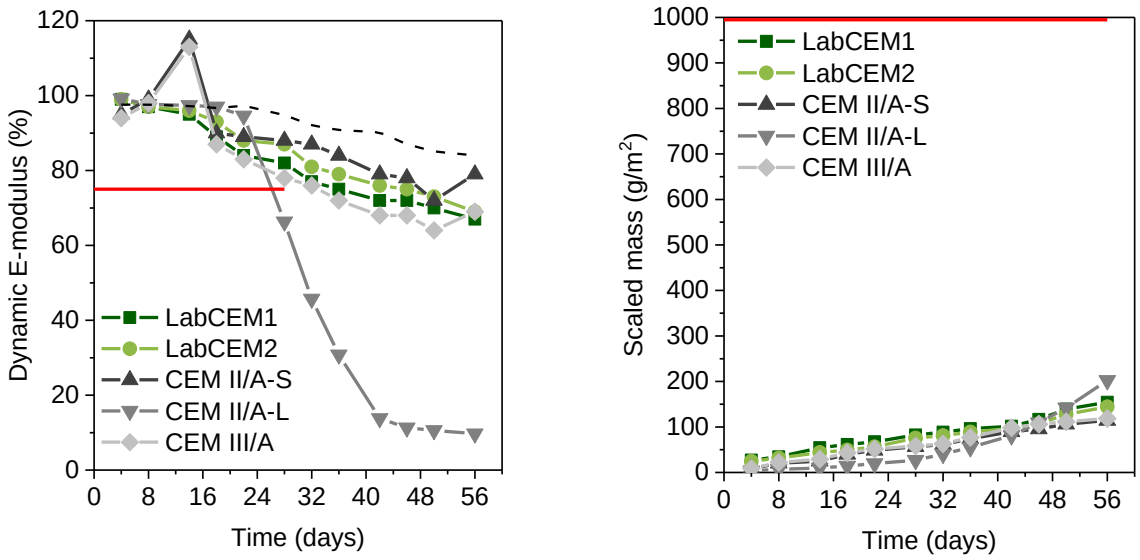

Figure 12 Evolution of the dynamic E-modulus and scaled material during the capillary suction and freeze-thaw testing (CF) The read lines gives the limits for the exposure resistance classes. The dashed line shows the results for concrete based on CEM I 52.5 R used for the preparation of the LabCems.

The resistance of the concretes to the freeze-thaw with de-icing salt was tested according to CDF (capillary suction, de-icing agent and freeze-thaw) test. The results are shown in Figure 13. All the tested concretes are characterized by a lower scaling than 1500 g/m^2 after 28 freeze-thaw cycling as required by (Setzer and Auberg, 1995).

The presented results agree well with the available literature data. Generally, the freeze-thaw performance of the cement containing slag is similar or inferior when compared to the neat Portland cements (CEM I) (Utgenannt and Petersson, 2010). This is often associated with fact that the carbonation resulting the opening of the microstructure of the slag cements white in the case of neat Portland cement it is initially densifying the microstructure (Zhang et al., 2017; Adu-Amankwah et al., 2017a). Limestone, when used at a higher replacement ratio, has a negative impact on the scaling resistance. For lower dosages, it has no pronounced impact (Palm et al., 2016) and the cements with limestone generally fulfil the requirements (Bolte and Zajac, 2016; Palm et al., 2016). These differences can be well explained with the help of the modelling results shown in the section "**Fehler! Verweisquelle konnte nicht gefunden werden. Fehler! Verweisquelle konnte nicht gefunden werden.**". The replacement of the clinker by the slag results in a reduction of the portlandite content and the increase of the C-S-H (Figure 6). Therefore, in the case of the slag this is the C-S-H phase that is more prone to carbonation, resulting in its shrinkage and opening of the microstructure (Chen et al., 2006; Morandeau et al., 2015). In the case of CEM I, the portlandite is mainly carbonating phase which results in the increase of the solid volume and decrease of the porosity. Figure 7 reveals that the increase of the limestone content over 10 % results in the increase of the total porosity volume and consequently in a less durable concrete.

The results of rapid chloride migration tests are shown in Figure 13. The penetration of chloride into the mortars is lower for the cements containing slag, when compared to the limestone cement and lower or similar to the CEM I. In general, the slag is improving the resistance of the cement mortars and concretes to the chloride migration because of the finer porosity, the higher chloride binding; both related to the

increase of the C-S-H content as shown in Figure 6. It also increases capacity to chemical binding because of the formation of the Friedel salt (Luo et al., 2003; Thomas et al., 2012). Thermodynamic modelling reveals that in the composition range investigated, the mechanism related to the microstructure densification and physical adsorption is dominating since the AFm phase content is similar for a given limestone content.

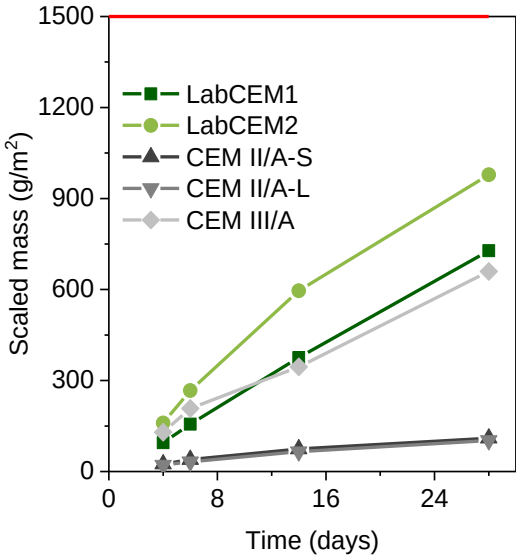

Figure 13 Evolution of the scaled material during the capillary suction, de-icing agent and freeze-thaw (CDF) The read lines gives the limits for the exposure resistance classes. The dashed line shows the results for concrete based on CEM I 52.5 R used for the preparation of the LabCems.

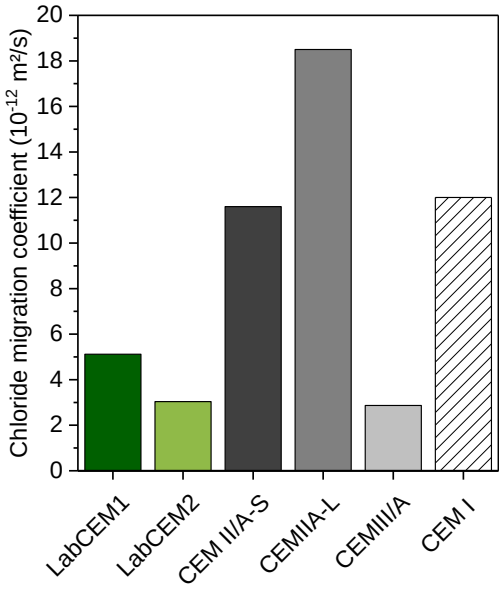

Figure 14 Rapid chloride migration coefficient determined at 28 days. Additionally the chloride migration coefficient is given for the same CEM I 52.5 R.

Overall, the investigation of the mortars and concretes performance reveal that the LabCem1 and LabCem2 are characterized by performance which is generally comparable to the CEM I used for the production of these cements. Some properties, namely the carbonation and scaling resistance, as worse while others, namely chloride resistance, are better. However, the performance of the optimized cement is comparable or superior to the cements currently available in market such as CEM II/A-S and CEM III/A, which are of the same strength class. Compared to these cements, the optimized cements offer a significant improvement of the effective global warming potential.

4. Conclusions

The production of the Portland cement clinker is associated with significant CO_2 emissions. The cement industry has already reached considerable reductions in the CO_2 emissions associated with cement production. These efforts need to be further followed to cope with the increasing demand for the cement. The quantities of the useful SCMs are limited and are unlikely to increase. Still, recent research work revealed that use of granulated blast-furnace slag in combination with limestone may lead to further

increase of the clinker replacement ratio while keeping the granulated blast-furnace slag content relatively low in cement.

The present contribution demonstrates an optimization tool for the composition of multicomponent cement enabling minimizing the Portland cement clinker and granulated blast-furnace slag content while maximizing the performance of the cement.

The impact of the initial cement composition on the phase assemblage and resulting porosity was investigated by means of the thermodynamic modelling supported by the hydration kinetics models. The approach used accounted for the specific interactions among the clinker, slag and limestone. Knowledge of the microstructure features in the investigate systems enabled the prediction of the compressive strength at different hydration times. The modelling predictions were verified by the testing of laboratory cements according to the existing standards. The general agreement between predictions and measured performance evolution had confirmed the accuracy of the models developed as well as of the general concept of the composite cement optimization. Consequently, the effective global warming potential of the composite cements could be calculated. This revealed that composite cements characterized by the approximatively 50 wt.-% of Portland cement clinker, 40 wt.-% of granulated blast-furnace slag and 10 wt.-% of limestone are characterized on one hand by the appreciable performance, on the other hand by the lowest effective global warming potential and generally low warming potential.

Since the prediction of the durability performance is currently not possible, this was tested. This investigation showed that the optimized cements are characterized by the durability performance comparable or superior to the commercial composite cements. These are, however, characterized by lower Portland cement clinker replacement ratio and hence associated with higher CO_2 emissions. The modelling results further provided valuable insights into the underlying phenomena that helped to analyze the experimental observations related to the concrete performance parameters.

It is important to note that the developed model is flexible with respect to the cement composition and its kinetics of the hydration. Any composition of the Portland cement clinker, granulated blast-furnace slag and limestone of the known hydration kinetics can be modelled and the performance predicted. This applies as well for the different supplementary materials, e.g. fly ash or calcined clay.

5. Acknowledgements

This project has received funding from the European Union's Horizon 2020 research and innovation program under grant agreement No 760639 “EnDurCrete”.

6. Literature

Adu-Amankwah, S., Zajac, M., Skocek, J., Ben Haha, M., Black, L., 2017a. Relationship between cement composition and the freeze–thaw resistance of concretes. Adv. Cem. Res. 1–11. https://doi.org/10.1680/jadcr.17.00138

Adu-Amankwah, S., Zajac, M., Stabler, C., Lothenbach, B., Black, L., 2017b. Influence of limestone on the hydration of ternary slag cements. Cem. Concr. Res. 100, 96–109. https://doi.org/10.1016/j.cemconres.2017.05.013

Alexander, M., Thomas, M., 2015. Service life prediction and performance testing — Current developments and practical applications. Cem. Concr. Res. https://doi.org/10.1016/j.cemconres.2015.05.013

Antoni, M., Baquerizo, L., Matschei, T., 2015. Investigation of Ternary Mixes Made of Clinker Limestone and Slag or Metakaolin: Importance of Reactive Alumina and Silica Content, in: Calcined Clays for Sustainable Concrete. Springer, pp. 545–553.

Berodier, E., Scrivener, K., 2015. Evolution of pore structure in blended systems. Cem. Concr. Res. 73, 25–35. https://doi.org/10.1016/j.cemconres.2015.02.025

Bolte, G., Zajac, M., 2016. Limestone requirements for high-limestone cements. ZKG Int. 69, 54–60.

Chen, J.J., Thomas, J.J., Jennings, H.M., 2006. Decalcification shrinkage of cement paste. Cem. Concr. Res. 36, 801–809. https://doi.org/10.1016/j.cemconres.2005.11.003

Damidot, D., Lothenbach, B., Herfort, D., Glasser, F.P., 2011. Thermodynamics and cement science. Cem. Concr. Res. 41, 679–695. https://doi.org/10.1016/j.cemconres.2011.03.018

De Weerdt, K., Haha, M.B., Le Saout, G., Kjellsen, K.O., Justnes, H., Lothenbach, B., 2011. Hydration mechanisms of ternary Portland cements containing limestone powder and fly ash. Cem. Concr. Res. 41, 279–291. https://doi.org/10.1016/j.cemconres.2010.11.014

Douglas Hooton, R., 2015. Current developments and future needs in standards for cementitious materials. Cem. Concr. Res. https://doi.org/10.1016/j.cemconres.2015.05.022

für Wasserbau, B., 2012. BAW-Merkblatt: Frostprüfung von Beton. Karlsruhe.

Gartner, E., Hirao, H., 2015. A review of alternative approaches to the reduction of CO2 emissions associated with the manufacture of the binder phase in concrete. Cem. Concr. Res. 78, 126–142. https://doi.org/10.1016/j.cemconres.2015.04.012

Hummel, Wolfgang, Berner, U., Curti, E., Pearson, F., Thoenen, T., 2002. Nagra/PSI chemical thermodynamic data base 01/01. Radiochim. Acta 90, 805–813.

Hummel, W, Berner, U., Curti, E., Pearson, F., Thoenen, T., 2002. Nagra Technical Report NTB 02-16. Wettingen Switz.

Ishida, T., Luan, Y., Sagawa, T., Nawa, T., 2011. Modeling of early age behavior of blast furnace slag concrete based on micro-physical properties. Cem. Concr. Res. 41, 1357–1367.

Kocaba, V., Gallucci, E., Scrivener, K.L., 2012. Methods for determination of degree of reaction of slag in blended cement pastes. Cem. Concr. Res. 42, 511–525. https://doi.org/10.1016/j.cemconres.2011.11.010

Kucharczyk Sylwia, Deja Jan, Maciej Zajac, 2016. Effect of slag reactivity influenced by alumina content on hydration of composite cements. J. Adv. Concr. Technol. 4, 535–547. https://doi.org/doi:10.3151/jact.14.535

Kulik, D.A., Wagner, T., Dmytrieva, S.V., Kosakowski, G., Hingerl, F.F., Chudnenko, K.V., Berner, U.R., 2013. GEM-Selektor geochemical modeling package: revised algorithm and GEMS3K numerical kernel for coupled simulation codes. Comput. Geosci. 17, 1–24.

Kunther, W., Lothenbach, B., Scrivener, K.L., 2013. On the relevance of volume increase for the length changes of mortar bars in sulfate solutions. Cem. Concr. Res. 46, 23–29.

Lothenbach, B., Kulik, D., Matschei, T., Balonis, M., Baquerizo, L., Dilnesa, B.Z., Miron, D., Myers, R.E., 2018. Cemdata18: A thermodynamic database for hydrated Portland cements and alkali-activated materials. Cem. Concr. Res.

Lothenbach, B., Le Saout, G., Gallucci, E., Scrivener, K., 2008a. Influence of limestone on the hydration of Portland cements. Cem. Concr. Res. 38, 848–860. https://doi.org/10.1016/j.cemconres.2008.01.002

Lothenbach, B., Matschei, T., Möschner, G., Glasser, F.P., 2008b. Thermodynamic modelling of the effect of temperature on the hydration and porosity of Portland cement. Cem. Concr. Res. 38, 1–18. https://doi.org/10.1016/j.cemconres.2007.08.017

Lothenbach, B., Scrivener, K., Hooton, R.D., 2011. Supplementary cementitious materials. Cem. Concr. Res. 41, 1244–1256.

Lothenbach, B., Winnefeld, F., 2006. Thermodynamic modelling of the hydration of Portland cement. Cem. Concr. Res. 36, 209–226. https://doi.org/10.1016/j.cemconres.2005.03.001

Luo, R., Cai, Y., Wang, C., Huang, X., 2003. Study of chloride binding and diffusion in GGBS concrete. Cem. Concr. Res. 33, 1–7.

Maddalena, R., Roberts, J.J., Hamilton, A., 2018. Can Portland cement be replaced by low-carbon alternative materials? A study on the thermal properties and carbon emissions of innovative cements. J. Clean. Prod. 186, 933–942. https://doi.org/10.1016/j.jclepro.2018.02.138

Morandeau, A., Thiéry, M., Dangla, P., 2015. Impact of accelerated carbonation on OPC cement paste blended with fly ash. Cem. Concr. Res. 67, 226–236. https://doi.org/10.1016/j.cemconres.2014.10.003

Palm, S., Proske, T., Rezvani, M., Hainer, S., Müller, C., Graubner, C.-A., 2016. Cements with a high limestone content – Mechanical properties, durability and ecological characteristics of the concrete. Constr. Build. Mater. 119, 308–318. https://doi.org/10.1016/j.conbuildmat.2016.05.009

Salas, D.A., Ramirez, A.D., Rodríguez, C.R., Petroche, D.M., Boero, A.J., Duque-Rivera, J., 2016. Environmental impacts, life cycle assessment and potential improvement measures for cement production: a literature review. J. Clean. Prod. 113, 114–122. https://doi.org/10.1016/j.jclepro.2015.11.078

Schöler, A., Lothenbach, B., Winnefeld, F., Haha, M.B., Zajac, M., Ludwig, H.-M., 2017. Early hydration of SCM-blended Portland cements: A pore solution and isothermal calorimetry study. Cem. Concr. Res.

Schöler, A., Lothenbach, B., Winnefeld, F., Zajac, M., 2015. Hydration of quaternary Portland cement blends containing blast-furnace slag, siliceous fly ash and limestone powder. Cem. Concr. Compos. 55, 374–382. https://doi.org/10.1016/j.cemconcomp.2014.10.001

Scrivener, K.L., John, V.M., Gartner, E.M., 2018. Eco-efficient cements: Potential economically viable solutions for a low-CO2 cement-based materials industry. Cem. Concr. Res. 114, 2–26. https://doi.org/10.1016/j.cemconres.2018.03.015

Setzer, M.J., Auberg, R., 1995. Freeze-thaw and deicing salt resistance of concrete testing by the CDF method CDF resistance limit and evaluation of precision. Mater. Struct. 28, 16–31.

Skocek, J., Zajac, M., Stabler, C., Ben Haha, M., 2017. Predictive modelling of hydration and mechanical performance of low Ca composite cements: Possibilities and limitations from industrial perspective. Cem. Concr. Res. 100, 68–83. https://doi.org/10.1016/j.cemconres.2017.05.020

Termkhajornkit, P., Nawa, T., 2007. Composition of CSH in the Hydration Products of Fly Ash-Cement System. Spec. Publ. 242, 361–374.

The Cement Sustainability Initiative Environmental Product Declaration (EPD) [WWW Document], 2017. URL http://www.wbcsdcement.org/index.php/epd-tool-1

The Cement Sustainability Initiative [WWW Document], 2017. . Cem. Sustain. Initiat. CSI. URL https://www.wbcsdcement.org/

The ecoinvent Database [WWW Document], 2017. URL http://www.ecoinvent.org/database/database.html

Thomas, M.D.A., Hooton, R.D., Scott, A., Zibara, H., 2012. The effect of supplementary cementitious materials on chloride binding in hardened cement paste. Cem. Concr. Res. 42, 1–7. https://doi.org/10.1016/j.cemconres.2011.01.001

Utgenannt, P., Petersson, P.-E., Frost Resistance of Concrete Containing Secondary Cementitious Materials . Experience from Field and Laboratory Investigations. *Nordic Miniseminar "Freeze-thaw testing of concrete-input to revision of CEN test methods", Vedbćk* (2010): 75-90.

VDZ-Publikation, 2017. Zementindustrie im Überblick 2017 [WWW Document]. URL https://www.vdz-online.de/publikationen/zementindustrie-im-ueberblick/ (accessed 12.1.17).

Wagner, T., Kulik, D.A., Hingerl, F.F., Dmytrieva, S.V., 2012. GEM-Selektor geochemical modeling package: TSolMod library and data interface for multicomponent phase models. Can. Mineral. 50, 1173–1195.

Whittaker, M., Zajac, M., Ben Haha, M., Black, L., 2016. The impact of alumina availability on sulfate resistance of slag composite cements. Constr. Build. Mater. 119, 356–369. https://doi.org/10.1016/j.conbuildmat.2016.05.015

Whittaker, M., Zajac, M., Ben Haha, M., Bullerjahn, F., Black, L., 2014. The role of the alumina content of slag, plus the presence of additional sulfate on the hydration and microstructure of Portland cement-slag blends. Cem. Concr. Res. 66, 91–101. https://doi.org/10.1016/j.cemconres.2014.07.018

Zajac, M., Ben Haha, M., 2014. Experimental investigation and modeling of hydration and performance evolution of fly ash cement. Mater. Struct. 47, 1259–1269. https://doi.org/10.1617/s11527-013-0126-1

Zajac, M., Rossberg, A., Le Saout, G., Lothenbach, B., 2014. Influence of limestone and anhydrite on the hydration of Portland cements. Cem. Concr. Compos. 46, 99–108. https://doi.org/10.1016/j.cemconcomp.2013.11.007

Zajac, M., Skocek, J., Adu-Amankwah, S., Black, L., Ben Haha, M., 2018. Impact of microstructure on the performance of composite cements: Why higher total porosity can result in higher strength. Cem. Concr. Compos. 90, 178–192. https://doi.org/10.1016/j.cemconcomp.2018.03.023

Zhang, W., Na, S., Kim, J., Choi, H., Hama, Y., 2017. Evaluation of the combined deterioration by freeze–thaw and carbonation of mortar incorporating BFS, limestone powder and calcium sulfate. Mater. Struct. 50, 171.

List of symbols and abbreviations

Cement chemistry shorthand notation used in cement science is applied in this paper:

C = CaO, S = SiO_2, A = Al_2O_3, F = Fe_2O_3, M = MgO, H = H_2O, c = CO_2, $ = SO_3

The main anhydrous phases and hydrates in cementitious systems are summarized in the table below:

Alite	C_3S	Ca_3SiO_5
Belite	C_2S	Ca_2SiO_4
Aluminate	C_3A	$Ca_3Al_2O_6$
Ferrite	C_4AF	$4CaO{\cdot}Al_2O_3{\cdot}Fe_2O_3$
Calcium silicate hydrate	C-S-H	$xCaO{\cdot}SiO_2{\cdot}yH_2O$ (variable composition)
Portlandite	CH	$Ca(OH)_2$
Monocarbonate	C_4AcH_{11} (Mc)	$3CaO{\cdot}Al_2O_3{\cdot}CaCO_3{\cdot}11H_2O$
Hemicarbonate	$C_4Ac_{0.5}H_{11.5}$ (Hc)	$3CaO{\cdot}Al_2O_3{\cdot}0.5Ca(OH)_2{\cdot}0.5CaCO_3{\cdot}11H_2O$
Monosulfate	$C_4A\$H_{12}$ (Ms)	$3CaO{\cdot}Al_2O_3{\cdot}CaSO_4{\cdot}12H_2O$
Ettringite	$C_6A\$_3H_{32}$ (Et)	$3CaO{\cdot}Al_2O_3{\cdot}3CaSO_4{\cdot}32H_2O$